Influence of wheel speed during planar flow melt spinning on the microstructure and soft magnetic properties of $Fe_{68.5}Si_{18.5}B_9Nb_3Cu_1$ ribbons

M. Srinivas · B. Majumdar · D. Akhtar · A. P. Srivastava · D. Srivastava

Abstract The structure and soft magnetic properties of $Fe_{68.5}Si_{18.5}B_9Nb_3Cu_1$ (at.%) alloy ribbons produced through planar flow melt spinning at different wheel speeds viz. 34, 17 and 12 m/s have been investigated using X-ray diffraction, differential scanning calorimetry, transmission electron microscopy, vibrating sample magnetometer and positron lifetime spectroscopy. Amorphous ribbons formed with different wheel speeds manifested different enthalpy and activation energy of crystallization. The volume fraction of nanocrystalline phase, saturation magnetization and permeability are found to increase whereas coercivity is found to decrease with increasing wheel speed on annealing. A detailed analysis of positron lifetime spectra obtained from the as-spun ribbons has been used to rationalize the variation in microstructure and magnetic properties. The presence of larger number of defects at higher wheel speed increases the volume fraction of nanocrystalline phase on annealing which improves the soft magnetic properties.

Introduction

Nanocrystalline Fe–Si–B–Nb–Cu alloys [1] possess unique combination of soft magnetic properties such as high saturation magnetization, permeability, resistivity, Curie temperature and very low coercivity as compared to other traditionally available materials. These alloys are prepared by rapid solidification (melt spinning) to obtain an amorphous phase followed by controlled annealing (partial devitrification) so as to obtain nanocrystalline precipitates in the amorphous matrix. Detailed investigations have been carried out to understand the phenomena behind the occurrence of ultra soft magnetic properties in these materials [2].

It is well known that the processing at different wheel speeds during the melt spinning results in different ribbon thicknesses thereby affecting the cooling rate. This in turn alters the microstructure of the as-spun ribbons and influences the soft magnetic properties after nanocrystallization [3]. Recently the influence of wheel speed on the microstructure and soft magnetic properties of Fe–Zr–B–Cu [4] and Fe–Co–B–Nb–Cu [5] alloy systems has been reported. Paolo Allia et al. [6] and Knobel et al. [7] have correlated the magnetic permeability of melt spun Fe–Si–B–Nb–Cu ribbons with quenching rate and found that higher quenching rates change the kinetics of crystallization of amorphous phase which leads to the improvement of permeability. El Ghannami et al. [8] attributed the presence of preferentially oriented larger grains of Fe–Si nanocrystals at lower wheel speed to the poor soft magnetic properties in as-spun ribbons. Panda et al. [9] have observed that ribbon produced at lower wheel speed has high coercivity and low initial susceptibility. However, these studies did not attempt to explain the microstructural influence on the magnetic property behaviour due to different processing conditions.

Although it is known that the change of wheel speed/cooling rate leads to the formation of different initial disordered structure of amorphous phase, the evidence of such disordered structure is not fully explored. It is also not clear

M. Srinivas · B. Majumdar (✉) · D. Akhtar
Defence Metallurgical Research Laboratory,
Hyderabad 500058, India
e-mail: bhaskar@dmrl.ernet.in

A. P. Srivastava · D. Srivastava
Materials Science Division, Bhabha Atomic Research Centre,
Mumbai 400094, India

how the difference in the precursor amorphous phase structure affects the microstructure and soft magnetic properties after annealing. In this study we report the structure and soft magnetic properties of $Fe_{68.5}Si_{18.5}B_9Nb_3Cu_1$ alloy produced in amorphous state by planar flow melt spinning at different wheel speeds viz. 34, 17 and 12 m/s. The investigators have observed a higher glass forming ability for this composition as compared to $Fe_{73.5}Si_{13.5}B_9Nb_3Cu_1$ alloy which has been studied extensively. Moreover, this composition has near zero magnetostriction value [1] which will result in obtaining better soft magnetic properties. A detailed investigation has been carried out to evaluate the defect characteristics of the amorphous phase using Positron annihilation spectroscopy and correlate with microstructures and magnetic properties. Positron annihilation spectroscopy is a powerful tool for detecting the internal structure of the amorphous phase [10] and has been utilized to gather information regarding the free volume, concentration and size of positron trapping sites, etc. in amorphous structures.

Experimental

Continuous 10 mm wide ribbons of $Fe_{68.5}Si_{18.5}B_9Nb_3Cu_1$ alloy were produced through planar flow melt spinning process [11]. Each run was carried out by melting 30 g of the alloy in quartz crucibles having rectangular slit of 10×0.5 mm. Three different wheel speeds viz. 34, 17 and 12 m/s were employed keeping the melt temperature at 1250–1300 °C, nozzle wheel gap at 0.2 mm and ejection pressure at 9.8 kPa. Since the ambient condition has practically no effect on the structure, thermal stability and magnetic properties of these alloys [12], all experiments were conducted in air. The as-spun ribbons were annealed in a vacuum tubular furnace (5 mPa) at 550 °C for 1 h.

Structure of as-spun and annealed ribbons (free surface) was characterized using a X-ray diffractometer (XRD, PHILIPS PW 1830) with Cu Kα ($\lambda = 0.15405$ nm) radiation. A differential scanning calorimeter (DSC, DuPont 910) was used to evaluate the thermal stability and kinetics of the crystallization of the as-spun ribbons. A precision ion polishing system (PIPS) was employed for TEM sample preparation by thinning from both the sides of the ribbon. The microstructures were observed using a transmission electron microscope (TEM, JEOL 2000FX) and field emission scanning electron microscope (FESEM, ZEISS). Saturation magnetization ($4\pi M_s$) of the as-spun and annealed samples was obtained using vibrating sample magnetometer (VSM, ADE EV9) at a field of 400 kA/m. Coercivity of as-spun and annealed ribbons was measured using coercimeter (FÖSTER-KOERZIMET 1.095). The permeability was measured by using a B–H hysteresis loop tracer (Ferrites India Ltd.) at 50 Hz. Positron annihilation lifetime measurements of as-spun ribbons were carried out using a fast–fast coincidence spectrometer with Na^{22} as positron source in a sandwich configuration. The lifetime spectra ($\sim 10^6$ counts) were analyzed using the code POSITRONFIT.

Results and discussions

Structure and thermal stability

Figure 1 shows the average thickness of ribbon as a function of wheel speed. The fitted curve obtained from the regression analysis with a correlation factor (R^2) of 0.976 revealed that the thickness varies inversely with the wheel speed to the power of -0.58 which is in agreement with the reported value [13]. Figure 2 shows the XRD spectra of the ribbons at wheel speed of 34, 17 and 12 m/s revealing the formation of complete amorphous phase. DSC thermograms of the as-spun ribbons (Fig. 3) exhibit exothermic peaks, corresponding to the crystallization of amorphous phase. The onset of crystallization temperatures (T_x) of all the ribbons are within 549 ± 3 °C. As can be observed in Table 1, the enthalpy of crystallization calculated from the area under the exothermic peaks increases with wheel speed. However, enthalpy of 34 m/s ribbon is quite high as compared to that of 17 and 12 m/s ribbons. DSC thermograms were obtained at various heating rates (β), and the apparent activation energy of crystallization (ΔE) determined using the method of Kissinger [14] from the slope of a plot of $\ln(T^2/\beta)$ versus $1/T$, where T is the peak temperature in the DSC thermogram. Figure 4 shows the Kissinger plots for all as-spun ribbons and the estimated activation energies have been given in Table 1. It can be observed that the ΔE increases from 3.55 to 4.35 eV when the wheel speed decreases from 34 to 12 m/s.
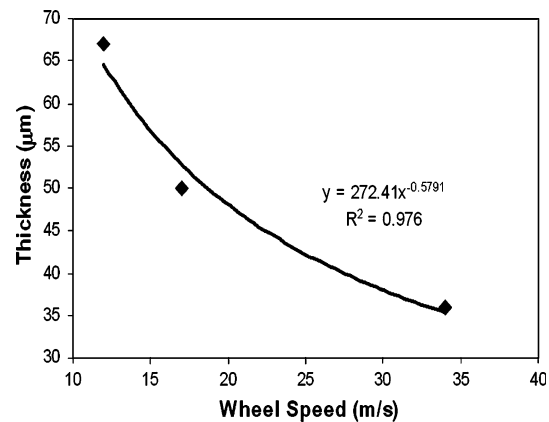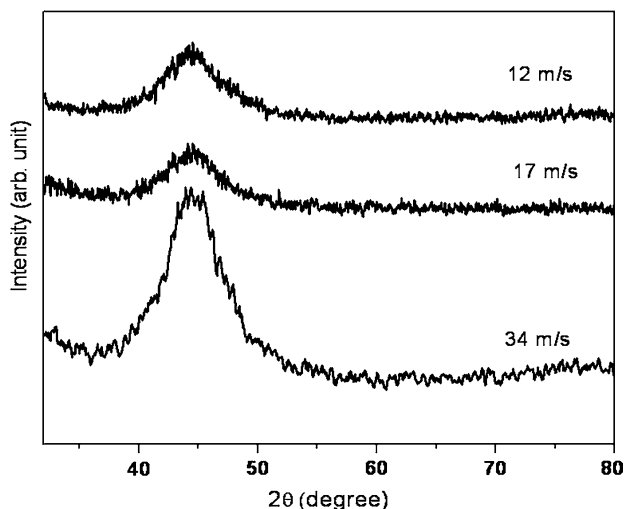

Fig. 1 Variation of ribbon thickness with wheel speed

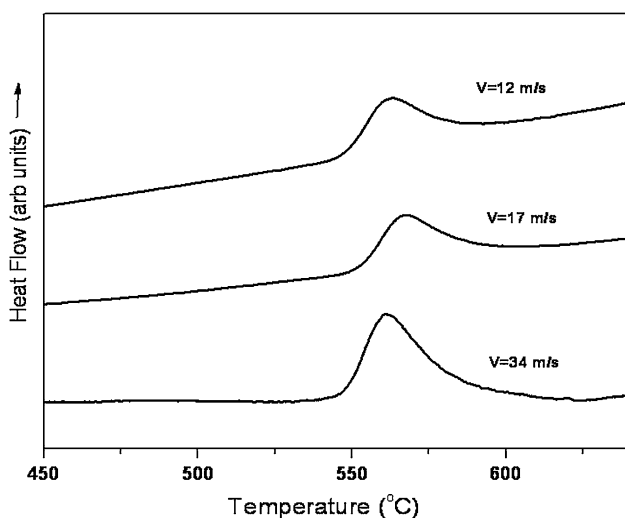Fig. 2 XRD patterns of as-spun ribbons at different wheel speeds

Fig. 4 Kissinger's plots of as-spun ribbons

Fig. 3 DSC thermograms of as-spun ribbons at different wheel speeds

Fig. 5 XRD patterns of ribbons annealed at 550 °C, 1 h

Microstructure

Figure 6a–c shows the TEM bright field images and corresponding selected area diffraction patterns of annealed ribbons (550 °C for 1 h) processed at different wheel speeds of 34, 17 and 12 m/s, respectively. Nanocrystalline Fe_3Si phase embedded in the amorphous matrix can be observed in all the samples which are in agreement with XRD observation. The grain size (d) measured from both TEM bright field and dark field images in an area of 500×600 nm for about 100–200 grains is included in Table 1 using method described elsewhere [15]. Though the grain size does not change significantly, the number of nanocrystalline grains is found to increase with wheel speed. The volume fraction of the nanocrystalline phase obtained from the field emission scanning electron microscopy (FESEM) images (Fig. 7)

Table 1 Crystallization data of melt spun alloy obtained at different wheel speeds

Wheel speed (m/s)	T_x (°C)	ΔH (W/g)	ΔE (eV)	d (nm)	V (%)
34	548	122	3.55	16	42
17	552	88	3.85	15	27
12	546	81	4.35	13	15

T_x crystallization temperature, ΔH enthalpy of crystallization, ΔE activation energy of crystallization, d grain size, V volume fraction of nanocrystals

XRD patterns of the ribbons annealed at 550 °C (just above the crystallization temperature) for 1 h shown in Fig. 5 indicate the presence of Fe_3Si phase in the amorphous matrix in all the samples.
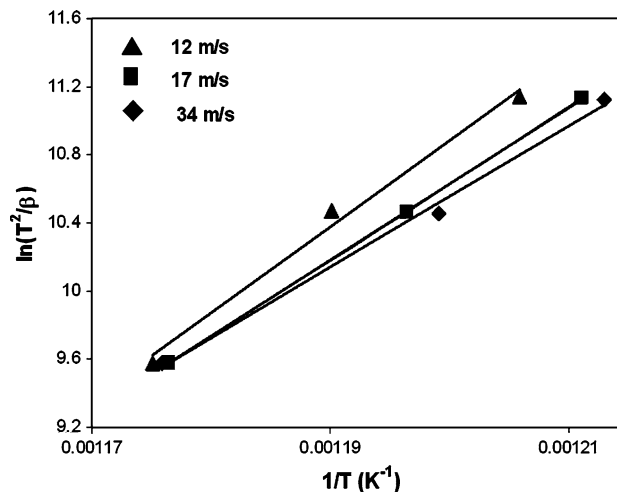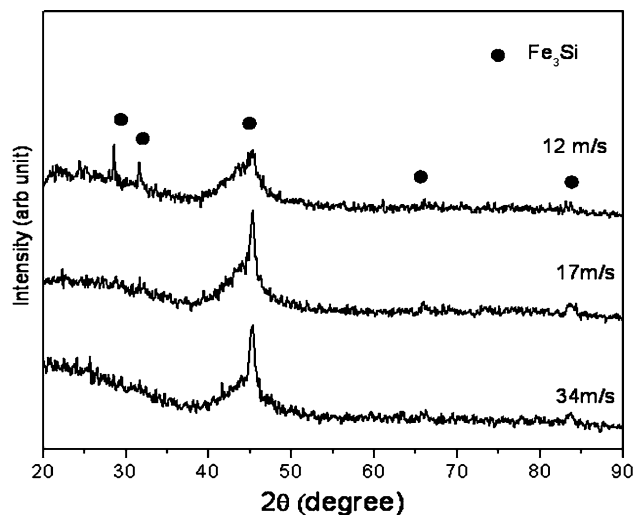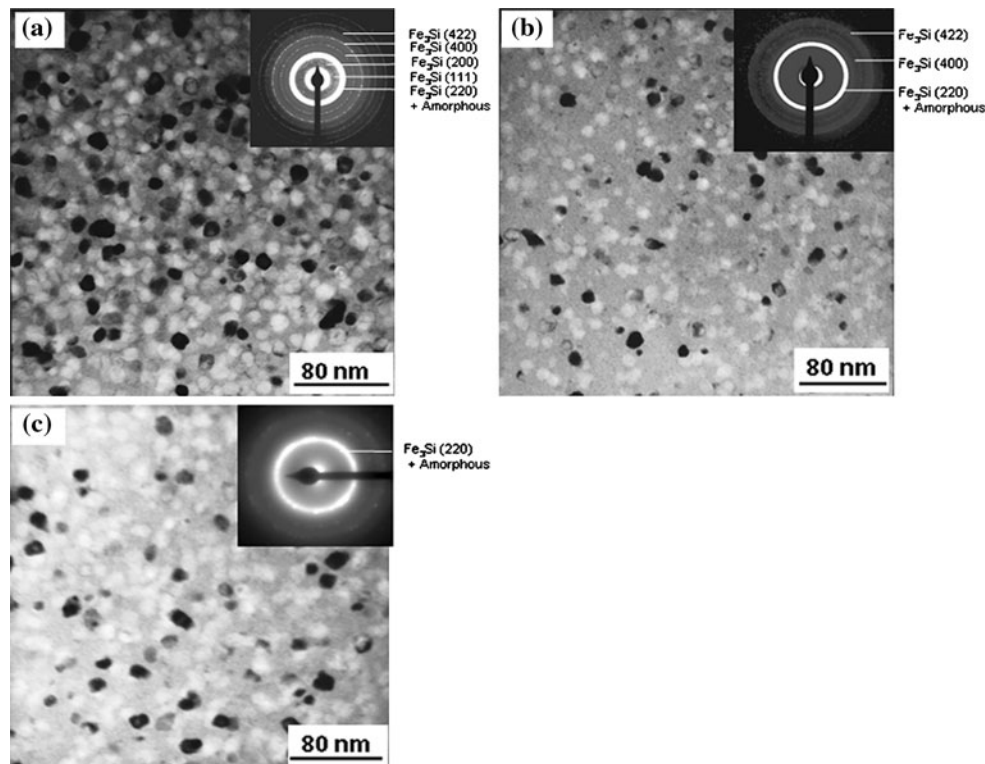
Fig. 6 TEM bright field image of ribbons produced at **a** 34 m/s, **b** 17 m/s and **c** 12 m/s and annealed at 550 °C, 1 h

using standard image analyzer is 42% in case of ribbons produced at 34 m/s whereas it decreases to 27% for 17 m/s and 15% for 12 m/s (Table 1).

Positron lifetime spectroscopy

The positron lifetime spectra of all the as-spun ribbons could be best fitted to two components with lifetime τ_1 and τ_2 having intensity of I_1 and I_2, respectively, using the code POSITRONFIT. The values of τ_1, τ_2, I_1 and I_2 for the ribbons produced at three different wheel speeds are given in Table 2. It can be observed that the small life component τ_1 is varying from 159 to 163 ps, similar to the value reported for positron lifetime in amorphous metallic ribbons [10]. Therefore, it can be concluded that the lifetime component τ_1 is due to the annihilation of positron in amorphous matrix. Small changes in τ_1 (161 ± 2 ps) confirmed that the nature of amorphous matrix is not changing significantly with variation in wheel speed. The long lifetime component τ_2 shows higher value and similar results have been reported [10] in different metallic glasses. Till recently only single lifetime component in amorphous metallic glass has been reported. But with the advances in techniques now it is possible to resolve the spectra into two components.

The long lifetime component is generally associated with the presence of appreciable number of quenched in

nuclei in groups, excess trapped vacancies, etc. in the form of cluster of structural free volumes (CSF) of amorphous state which is known to be a function of processing conditions [16]. In the present investigation, the intensity of τ_2 is found to be high for 34 m/s ribbon and it decreases with decreasing the wheel speed. This implies that large number of quenched in nuclei and high fraction of CSF (higher I_2) are present in 34 m/s wheel speed ribbon and reduce with decreasing the wheel speed/quenching rate. The results are in agreement with DSC and TEM investigations.

Magnetic properties

Figure 8 shows room temperature saturation magnetization ($4\pi M_s$) of the as-spun and annealed ribbons measured at a field of 400 kA/m as a function of wheel speed. It can be observed that saturation magnetization increases with wheel speed for both as-spun and annealed ribbons. However, the saturation magnetization values of annealed ribbons are lower than that of as-spun ribbons. These results are in agreement with those reported [17] earlier and may be attributed to the formation of ordered Fe_3Si phase which has lower saturation magnetization than amorphous phase. However, Fujii et al. [18] reported that in case of $Fe_{73.5}Si_{13.5}B_9Nb_3Cu_1$ alloy, the saturation value of the heat treated alloy is higher as compared to the amorphous state. Herzer [19] has reported the variation of the room
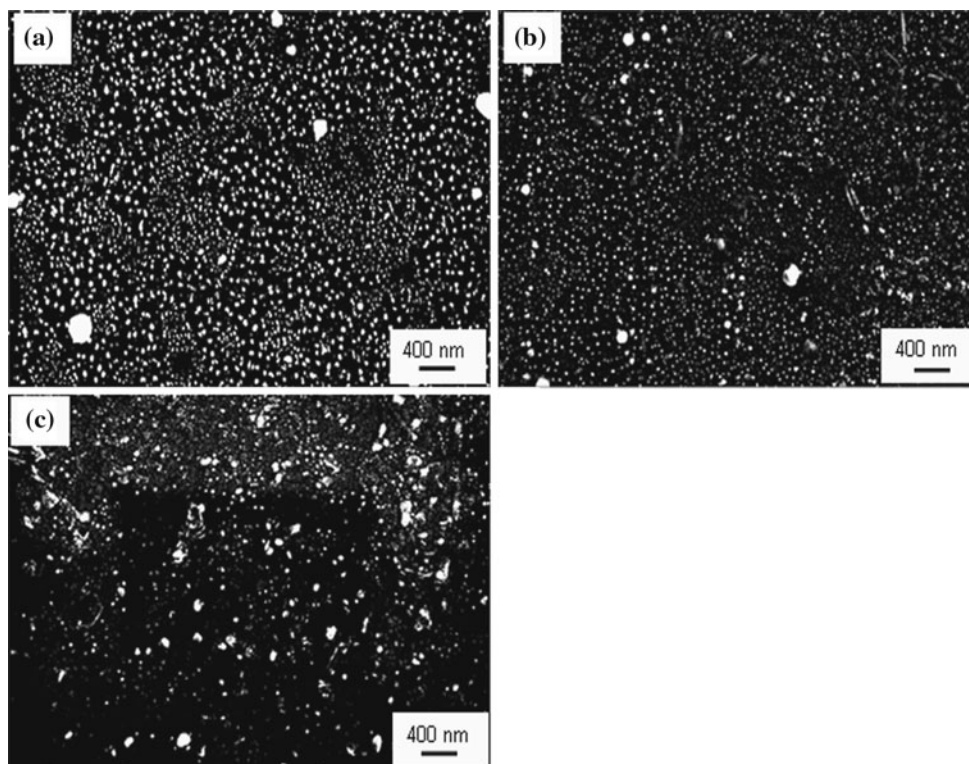
Fig. 7 FESEM images of ribbons produced at **a** 34 m/s, **b** 17 m/s and **c** 12 m/s and annealed at 550 °C, 1 h

Table 2 Positron annihilation data of ribbons processed at different wheel speeds

Wheel speed (m/s)	τ_1 (ps)	I_1 (%)	τ_2 (ps)	I_2 (%)
34	163	87.9	433	12.1
17	159	93.2	360	6.8
12	161	94.3	393	5.7

τ_1, τ_2 lifetime components of positron spectra, I_1, I_2 intensity of lifetime components τ_1 and τ_2, respectively
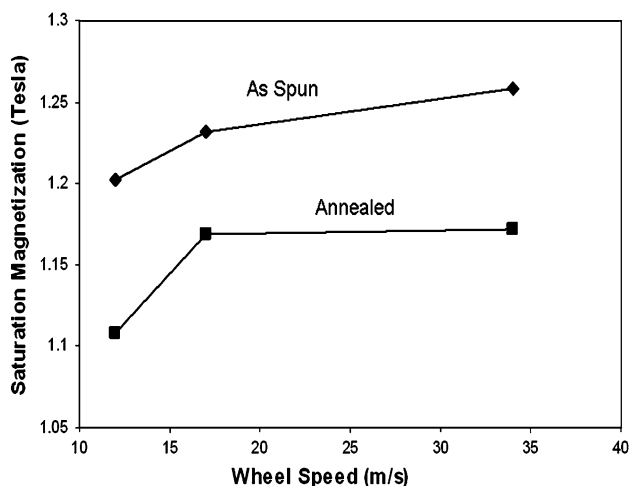

Fig. 8 Saturation magnetization of as-spun and annealed ribbons

temperature saturation magnetization of Fe–Si–B–Nb–Cu alloy as a function of Si content in both amorphous and nanocrystalline phase. It has been observed that at lower Si content, the saturation magnetization of nanocrystalline phase is quite high as compared to that of amorphous phase but decreases rapidly and cross-over takes place around 16 at.% Si. Therefore, in case of $Fe_{68.5}Si_{18.5}B_9Nb_3Cu_1$ alloy, containing 18 at.% Si, one can expect higher saturation magnetization values of as-spun ribbon (amorphous) as compared to the annealed ribbon containing nanocrystalline phase.

Figure 9 shows coercivity of the as-spun and annealed ribbons as a function of wheel speed. Coercivity of annealed ribbons is lower than that of as-spun ribbons. The coercivity is found to decrease with wheel speed, however, the decrease of coercivity for annealed ribbons is more pronounced. Figure 10 shows the variation of permeability for the as-spun and annealed ribbons with wheel speed. Permeability of annealed ribbons is higher than that of as-spun ribbons and it increases with wheel speed, the effect being more pronounced in annealed ribbons.

Soft magnetic properties of nanostructured Fe–Si–B–Nb–Cu alloys are attributed to the diminishing value of saturation magnetostriction (λ) and average magnetocrystalline anisotropy ($\langle K \rangle$). The effective magnetostriction (λ_{eff}) can be minimized by nullifying the positive
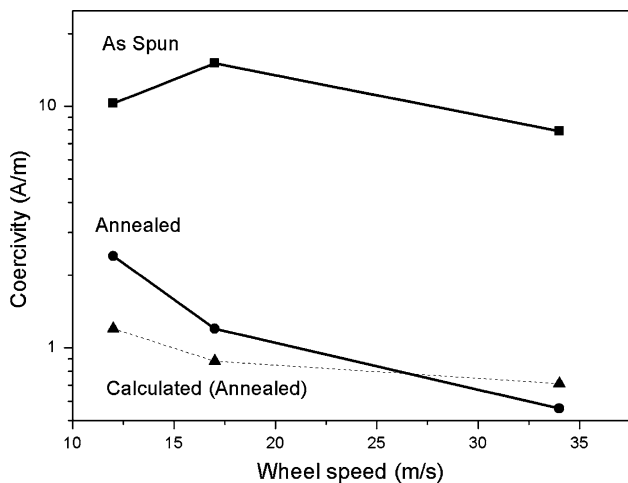
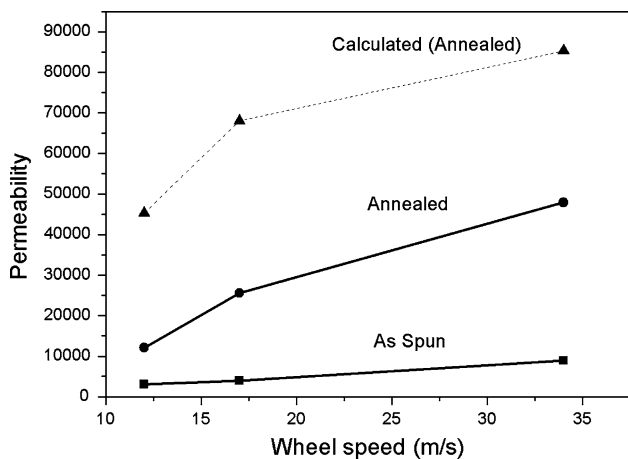**Fig. 9** Variation of coercivity of as-spun and annealed ribbons with wheel speed

Fig. 10 Variation of permeability of as-spun and annealed ribbons with wheel speed

magnetostriction of the residual amorphous matrix ($\lambda_{amor} = 20 \times 10^{-6}$) with the negative contribution of α-Fe(Si) nanocrystalline phase ($\lambda_{nc} = -6 \times 10^{-6}$) [20] in such a way that

$$\lambda_{eff} = (1 - v)\lambda_{amor} + v\lambda_{nc} = 0 \quad (1)$$

Our results indicate that the volume fraction of nanocrystalline phase increase with the wheel speed in annealed ribbons resulting in decreasing the value of λ_{eff}. This leads to the reduction of coercivity and enhancement of permeability of annealed ribbons progressively at higher wheel speeds as compared to the fully amorphous as-spun ribbons.

It is well established that under the application of magnetic field, the exchange coupling between nanocrystals and amorphous phase takes place causing averaging out of magnetocrystalline anisotropy and the exchange interaction forces the magnetization vector to be aligned

over several grains along field direction [21]. Accordingly the effective anisotropy (K_{eff}) can be given as

$$K_{eff} = \frac{\langle K \rangle}{\sqrt{N}} \quad (2)$$

where N is the number of grains of diameter D within the exchange length L_{ex} and can be expressed as

$$N = v\left(\frac{L_{ex}}{D}\right)^3 \quad (3)$$

It is evident that as the volume fraction (v) and number of grains increases the mangetocrystalline anisotropy decreases from 8 kJ/m^3 to few J/m^3. It is to be noted that the scale of exchange interaction expands to about 2 μm [19] during magnetization, thereby decreasing the effective anisotropy of the material. Coercivity (H_c) and permeability (μ_i) of the nanocrystalline alloys are quantitatively related to K_{eff} by [20]

$$H_c = p_c \frac{K_{eff}}{M_s} \quad (4)$$

$$\mu_i = p_u \frac{M_s^2}{\mu_o K_{eff}} \quad (5)$$

where p_c (=0.13) and p_u (=0.5) are dimensionless prefactors.

The coercivity and permeability values of annealed ribbons as a function of wheel speed have been estimated quantitatively and included in Figs. 9 and 10, respectively. It can be observed that trends in calculated and experimental values for both coercivity and permeability are same. In fact the calculated coercivity values almost coincide with the experimental values. However, in case of permeability, low experimental values may be attributed to the surface quality of the ribbons.

Conclusions

1. Amorphous ribbons produced at higher wheel speed during melt spinning exhibit higher enthalpy of crystallization revealing that energy entrapped in the sample in the form of defects and structural free volume is higher. This is supported by the positron lifetime spectroscopy observations where higher fraction of CSF was found in 34 m/s ribbon.

2. Lower activation energy of crystallization for ribbons prepared at high wheel speed suggests the ease of relaxation kinetics resulting in higher rate of nucleation. This is reflected by the TEM images where volume faction of nanocrystalline phase after annealing at the same temperature and time is higher.

3. The saturation magnetization increases with wheel speed for both as-spun and annealed ribbons. However,

the saturation magnetization values of annealed ribbons are lower than that of as-spun ribbons. This can be attributed to the formation of low saturation Fe_3Si nanocrystalline phase.

4. The decrease of coercivity and increase of permeability with wheel speed is due to the increase of volume fraction of nanocrystalline phase which reduces effective anisotropy (K_{eff}) and magnetostriction (λ_{eff}).

5. Quantitative estimation of coercivity and permeability of annealed ribbons as a function of wheel speed is found to be in agreement with the experimentally observed values.

References

1. Yoshizawa Y, Yamauchi K (1989) Hitachi Metals Ltd, Tokyo EU Patent no. 0299498
2. Yoshizawa Y, Oguma S, Yamauchi K (1988) J Appl Phys 64:6044
3. Takayama S, Oi T (1979) J Appl Phys 50:1595
4. Arvindha Babu D, Majumdar B, Sarkar R, Akhtar D, Chandrasekaran V (2008) J Phys D 41:195002
5. Arvindha Babu D, Srivastava AP, Majumdar B, Srivastava D, Akhtar D (2010) Metall Mater Trans A 41:1313
6. Allia P, Tiberto P (1994) IEEE Trans Magn 30:461
7. Knobel M, Sinnecker JP, Saenger JF, Sato Turtelli R (1993) Philos Mag B 68:861
8. El Ghannami M, Kulik T, Hernando A, Fernandez Barquin L, Gomez Sal JC, Gorria P, Barandiaran JM (1994) J Magn Magn Mater 133:314
9. Panda AK, Roy S, Singh SR, Rao V, Pramanik S, Chattoraj I, Mitra A, Ramchandrarao P (2001) Mater Sci Eng A 304–306:457
10. Gopinathan KP, Sundar CS (1984) In: Anantharaman TR (ed) Metallic glasses: production, properties and applications. Trans Tech Publications, Switzerland
11. Narasimhan MC, Flanders NJ (1979) US Patent no. 4142571
12. Majumdar B, Akhtar D (2005) Bull Mater Sci 28:395
13. Tkatch VI, Limanovskii AI, Denisenko SN, Rassolov SG (2001) Mater Sci Eng A 323:91
14. Kissinger HE (1957) Anal Chem 29:1702
15. Majumdar B, Bysak S, Akhtar D (2007) J Magn Magn Mater 309:300
16. Srivastava AP, Srivastava D, Dey GK, Sudarsan K, Pujari PK (2009) Metall Mater Trans A 40:1757
17. Locvas A, Kiss LF, Balogh I (2000) J Magn Magn Mater 215–216:463
18. Fujii H, Yardley VA, Matsuzaki T, Tsurekawa S (2008) J Mater Sci 43:3837 10.1007/s10853-007-2220-7
19. Herzer G (1997) In: Buschow KHJ (ed) Handbook of magnetic materials, vol 10. Elsevier Science B.V., p 415
20. Herzer G (1991) Mater Sci Eng A 133:1
21. Alben R, Becker JJ (1978) J Appl Phys 47:1653